Title	Numerical Analysis of the Effect of Sulfur Content upon Fluid Flow and Weld Pool Geometry for Type 304 Stainless Steel(Physics, Processes, Instruments & Measurements)
Author(s)	Lei, Yongping; Shi, Yaowu; Murakawa, Hidekazu et al.
Citation	Transactions of JWRI. 1997, 26(1), p. 1-8
Version Type	VoR
URL	https://doi.org/10.18910/11159
rights	
Note	

Numerical Analysis of the Effect of Sulfur Content upon Fluid Flow and Weld Pool Geometry for Type 304 Stainless Steel[†]

Yongping LEI[*], Yaowu SHI[**], Hidekazu MURAKAWA[***] and Yukio UEDA[****]

Abstract

In this paper, the effects of sulfur content on the thermocapillary convection in weld pools and the pool shapes of type 304 stainless steel for gas tungsten arc (GTA) welding process have been simulated numerically using a one-region continuum model. A newly developed model for calculating the influence of sulfur on surface tension temperature coefficients has been used. The condition for the computations are; sulfur contents from 0.003 to 0.03 weight percent, 100A welding current, and a normal gravity environment. The predicted results indicated that if the sulfur content is below about 0.015%, the flow is characterized by two opposite rotating vortexes and a singular velocity at the collision point between outward and inward flows on the weld pool surface, where the sign of the surface tension temperature coefficient changes from a positive to negative value. One vortex, driven by the positive surface-tension temperature coefficient, has a high strength, and the other, driven by the negative surface tension temperature coefficient, has a relatively weak strength. The inward flow develops with an increase of sulfur content, and eventually envelops the entire molted pool, and results in a deep penetration. The outward flow gradually becomes weaker and finally disappears. Meanwhile, the singularity of surface velocity is decreased simultaneously.

KEY WORDS: (Welding Pool) (Fluid Flow) (Active Element) (Surface Tension) (Vaporization)

1. Introduction

In recent years, there have been extensive studies to develop mathematical methods to predict the influence of physical variables and welding parameters on the transport phenomena occurring during welding processes[1-16]. These theoretical investigations have indicated that there exist four types of distinct driving force, *i.e.*, electromagnetic force, buoyancy force, thermocapillary force and aerodynamic drag force (arc drag) acting on the liquid metal in the weld pool. Most studies on convection heat and fluid flow have revealed that thermocapillary force is the dominant driving force which determines circulation in the weld pool. These thermocapillary forces, which give rise to the thermocapillary (Marangoni) convection, are known as the result of surface tension gradients on the weld pool surface.

In early theoretical investigations of weld pool convection, the value of the surface tension gradient was assumed to be constant in both gas metal and gas tungsten arc welding systems[6,8,9], and not dependent on the local temperatures nor the concentration of surface active elements such as sulfur throughout the range of temperature experienced during welding, except for Zacharia *et al.*[3,4] and Choo *et al.*[14,15]. To a large extent, the assumption of constant surface tension temperature gradients comes from the lack of accurate relationships among the surface tension temperature coefficient, temperature and amount of surface active element in the weld metal.

Heiple *et al.*[17-22] have made a series of experimental studies to investigate the effect of surface active elements on the weld pool penetration. Their results indicated that small changes of surface active elements (S) can significantly alter the surface tension of the weld metal, thereby producing appreciable variations in weld penetration. Hinata *et al.*[23] have experimentally

investigated the effect of sulfur on the aspect ratio of the GTA weld pool for 304 stainless steel. Scheller et al.[24] have also experimentally studied the influence of sulfur and welding condition on penetration in thin strip stainless steel. Their results indicated that the temperature coefficient of surface tension changes from negative to positive when the sulfur content reaches a critical value, and the weld penetration increases with increasing sulfur content. The values of the temperature coefficient of surface tension, $\partial r/\partial T$, calculated using an equation proposed by McNallan and Debroy[25], are in excellent agreement with the values recorded experimentally for 18Cr8Ni stainless steel in the temperature ranges of 1550-1800 °C, especially when probable uncertainties involved in S analyses (5ppm) are taken into account. Sahoo, Debroy and McNallan[26] were the first to develop a semi-empirical relationship between the surface temperature and concentration of surface active element and demonstrated that the surface tension of many binary metal-surface active solute systems can be adequately modeled on the basis of the Gibbs and Langmuir adsorption isotherm with consideration of the surface segregation of the solutes. Most of their calculated values compared very well with experimental results.

Zacharia[3,4] used the model proposed by Sahoo et al. as a submodel for calculation of the surface tension temperature coefficient of type 304 stainless steel. The surface tension temperature coefficient is assumed to be a function of the surface temperature and concentration of the surface active element, so as to simulate the influence of the thermocapillary convection on the weld pool geometry. Their calculated results clearly revealed that when the sulfur content is equal to 0.024%, there are two circulation cells in each half of the weld pool, but they did not show the velocity and temperature distribution on the weld pool surface. Choo and Szekely[14,15] have also used this model to calculate the weld pool shapes, surface velocity and temperature for 304 stainless steel under the conditions of a vaporization submodel combining a Langmuir kinetic vaporization mechanism with mass transfer from the pool. Their predicted results did not indicate a singular peak velocity and great temperature drops at certain regions on the weld pool surface.

The purpose of the present paper is to predict the influence of sulfur content of weld metal on the weld pool shapes and surface phenomena by numerical computation considering the variation of the surface tension temperature coefficient. A type 304 stainless steel system was chosen for the present investigation, since the alloy has been the subject of a number of computational as well as experimental studies. A newly developed surface tension model[26] was utilized to evaluate the variation of $\partial \gamma/\partial T$ as a function of temperature and content of surface active element.

2. Model and Governing Equations

In order to clarify the influence of sulfur contents on weld pool penetration and geometry as well as the temperature and velocity distribution on the weld pool surface, the stationary gas tungsten arc (GTA) welding process is chosen as an example and shown schematically in Fig.1. Three distinct regions, that is a solid region, a mushy region consisting of liquid dispersal within the solid dendrites and a total liquid region, appear during the welding process. To develop a numerical model, the following major assumptions have been made.

1) The heat transfer and fluid flow in the weld pool are adequately described by axisymmetric, time dependent representations;

2) Heat and current flux from the arc to the anode (metal) surface is a specified symmetric Gaussian distribution;

3) Surface tension force, buoyancy force and electromagnetic force are the driving forces acting on the molten metal;

4) Thermophysical properties are constant but their value may be different in solid and liquid regions, and Boussinesq approximation is used;

5) The weld pool surface is assumed flat, and this is reasonable in view of the lower welding current (100A)

On the above assumptions, a set of one-region continuum equations describing the total mass, momentum and energy conservation for unsteady heat and
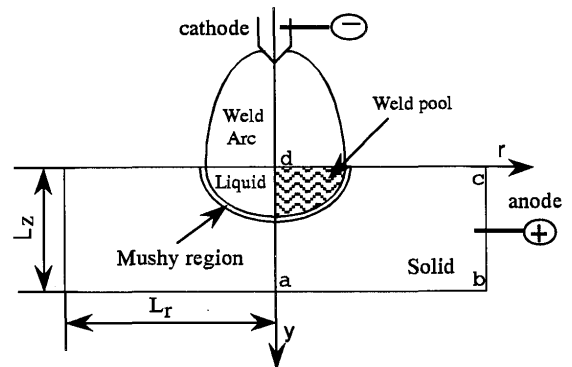

Fig.1 Schematic illustration of the stationary GTA welding Process. The computational domain is represented by abcd region.

fluid flow in liquid, solid and mushy regions can be expressed in cylindrical coordinates. The formulations can be found in detail in the reference[27], but in the present calculations the electromagnetic force has been taken into account as a driving force of liquid motion in weld pool. Therefore, the electromagnetic force, $-J_z B_\theta$ and $J_r B_\theta$, should be included in the source terms of radial and axial momentum equations, respectively. The current density components J_r, J_z and the magnetic flux component B_θ are given in the following forms,

$$J_z = \frac{I}{2\pi} \int_0^\infty \lambda J_0(\lambda r) \exp(-\lambda z - \lambda^2 r_e^2/12) \, d\lambda \qquad (1)$$

$$J_r = \frac{I}{2\pi} \int_0^\infty \lambda J_1(\lambda r) \exp(-\lambda z - \lambda^2 r_e^2/12) \, d\lambda \qquad (2)$$

$$B_\theta = \frac{\mu_m I}{2\pi} \int_0^\infty J_1(\lambda r) \exp(-\lambda z - \lambda^2 r_e^2/12) \, d\lambda \qquad (3)$$

where I is the welding current, μ_m is the magnetic permeability of free space, θ is the third independent variable in the cylindrical coordinate system, J_0 and J_1 are the first order Bessel functions of the zero kind and of the first kind, respectively.

3. Boundary conditions

The model considers the heat flux from the arc at the top surface of the workpiece as a specified symmetric Gaussian distribution described by:

$$q_{arc} = \frac{3IE}{\pi r_b^2} \exp\left(\frac{-3r}{r_b^2}\right) \qquad (4)$$

where E is welding voltage and r_b is effective radius of heat flux distribution.

At the top surface of the workpiece, the heat loss by convection heat transfer, the radiation heat transfer and the vaporization of alloying elements have been taken into account, and it is given by

$$q_{loss} = h_c(T - T_a) + \sigma_b e(T^4 - T_a^4) + \sum J_i L_{vap,i} \qquad (5)$$

where h_c is the convection heat transfer coefficient, σ_b is the Stefan-Bolzmann constant, e is the emissivity, $L_{vap,i}$ is the heat of vaporization of species i, and T_a is ambient temperature. The vaporization rate of alloy elements i, J_i, is calculated using the Langmuir equation and given by

$$J_i = \frac{M_i p_i}{\sqrt{2\pi M_i \, RT}} \qquad (6)$$

where M_i is the atomic weight of species of i, R is the gas constant, p_i is the partial pressure of species i.

This relationship assumes that there is no impediment to the alloying elements leaving the weld pool surface. It is correct for the vaporization into a perfect vacuum. In practice, the GTA welding process is performed under the condition of atmospheric pressure. Therefore, the vaporization rate calculated by Eq.(6)

would be higher than that expected under actual conditions. Recently, Choo and Szekely[14] have developed a mixed control vaporization model in which both Langmuir vaporization and mass diffusion crossing the concentration boundary layer on the weld pool surface have been taken into account. Their calculated results show that the effective mass transfer coefficient (for Fe, Mn) is much less than that estimated by the Langmuir vaporization model. In order to illustrate the effects of mixed control vaporization using this method, the velocity of the plasma gas at the boundary layer on the pool surface must be known *a priori*. Because an arc model for calculating the arc thermophysical parameter fields has not been included in the present study, a constant coefficient that is equal to 30% of the mass loss calculated by the Langmuir equation has been introduced.

The p_i is evaluated following the method developed by Block-Bolten and Eagar[28],

$$\log p_i = \log a_i + \log p_i^0 \qquad (7)$$

where a_i is the activity of element i, p_i^0 is the equilibrium vapor pressure of pure element i at T. Thus, the net heat flux on the weld pool surface is

$$q_{net} = q_{arc} - q_{loss} \qquad (8)$$

At the surface of the workpiece, other than that of the weld pool, the convection heat transfer and radiation heat losses for the atmospheric cooling are given by

$$q_{srf} = h_c(T - T_a) + \sigma_b e(T^4 - T_a^4) \qquad (9)$$

The moving solid/liquid interface, which is an important feature to consider, is automatically determined by the liquid fraction field in the present computational algorithm.

On the free liquid surface of the weld pool, the temperature gradient along the radial direction produces a surface tension gradient and then induces fluid flow parallel to the surface from a region of higher surface tension to one of lower surface tension. Sahoo et al.[26] have demonstrated that the surface tension of many binary metal-surface active solute systems can be expressed as a function of both temperature and activity of the solute on the basis of Gibbs and Langmuir adsorption isotherms considering the surface segregation of the solute, and can be given by an equation as follows:

$$\gamma(T) = \gamma_{ref} - A(T - T_{ref}) - R T \Gamma_s \cdot \ln(1 + K_{seg} a_i)$$

$$K_{seg} = k_1 \exp\left(\frac{-\Delta H^0}{RT}\right) \qquad (10)$$

where γ_{ref} is the surface tension of pure metal in N/m at a reference temperature T_{ref}. A is a constant that expresses the variation of surface tension of pure metal at temperatures above the melting point in N/ (m-K), Γ_s is

the entropy factor, and ΔH^0 is the enthalpy of segregation.

Because of the continuity restriction at the weld pool surface, the change rate of surface tension along the radial direction must be balanced by the shear stress and can be formulated as

$$\tau = -\mu\left(\frac{\partial u}{\partial r}\right) = \left(\frac{\partial \gamma}{\partial T}\right)\left(\frac{\partial T}{\partial r}\right) \tag{11}$$

The temperature coefficient $\left(\partial \gamma / \partial T\right)$ can be obtained by differentiating Eq.(10) with respect to T with taking into account the activity of surface active element, a_i. It can be expressed as a function of temperature, i.e.

$$\frac{\partial \gamma}{\partial T} = -A - R\Gamma_i \cdot \ln(1 + K_{seg}a_i)$$
$$- \frac{K_{seg}a_i}{1 + K_{seg}a_i}\frac{\Gamma_i \Delta H^0}{T} - \frac{RT\Gamma_i K_{seg}}{1 + K_{seg}}a_i'(T) \tag{12}$$

where $a_i'(T)$ is the derivative of activity of surface active element with respect to T. Generally speaking, Eq.(10) and Eq.(12) are merely suitable for binary metal system. For mild steels, sulfur and oxygen are the most important surface elements commonly found. Therefore, it can be adequately treated as a pure metal. However, the investigation by McNallan and Debroy[25] has shown that the substantial quantities of the alloy elements contained in many engineering alloys, such as type 304 stainless steel, can also have a significant influence on the surface tension of the weld pool, as well as the temperature coefficient of surface tension, and as a consequence, on the weld pool convection. They have suggested that several issues should be considered for application of Eq.(10) to Fe-Cr-Ni systems when sulfur is the primary surface active impurity in the alloy. Based on thermodynamic calculations, their studies showed that in the case of type 304 stainless steel all of the variables in Eq.(10) can be given the same values as the Fe-S system, except for the activity of sulfur.

The influence of Cr and Ni on the activity of S can be expressed by the activity coefficient of S in liquid iron through their interaction parameters,

$$\log f_s = e_s^{Cr}[pct\ Cr] + r_s^{Cr}[pct\ Cr]^2$$
$$+ e_s^{Ni}[pct\ Ni] + r_s^{Ni}[pct\ Ni]^2 \tag{13}$$

The first- and the second-order interaction coefficients for the Fe-Cr-Ni-S system can be expressed respectively, as follows,

Interaction of Cr with S in iron

$$e_s^{Cr} = -94.2/T + 0.0394$$
$$r_s^{Cr} = 0 \tag{14}$$

Interaction of Ni with S in iron

$$e_s^{Ni} = 0$$
$$r_s^{Ni} = 0 \tag{15}$$

Substituting Eq.(14) and (15) into Eq.(13), a_s and $a_s'(T)$ in Eq.(12) are given by

$$a_s = [pct\ S] \cdot 10^{(e_s^{Cr}[pct\ Cr])} \tag{16}$$

$$a_s'(T) = [pct\ S] \cdot [pct\ Cr]10^{(e_s^{Cr}[pct\ Cr])} \cdot \frac{216.9}{T^2} \tag{17}$$

4. Numerical method

In the present study, the discretized equations were solved iteratively for each time increment using a control volume finite difference procedure. A fully implicit formulation is used for time-dependent terms, and power-law scheme is employed to evaluate the combined convection/diffusion coefficient. The SIMPLE algorithm is applied to solve the momentum and continuity equations to obtain the velocity field. The overall solution process is separated into two-steps. In the first step, an outer Newton linearization of source terms in the energy equation is used to linearize the enthalpy with respect to the current values. The second step is the inner solution of linear equations. It is solved iteratively within the internal nodes of the domain applying the line-by-line tridiagonal matrix algorithm (TDMA) and block correction technique. For each time increment, convergence is decided to be satisfied when the maximum of residual source of mass at the end of each iteration is less than 1.0×10^{-6}, and the maximum of absolute values of the relative difference in nodal enthalpy between successive iterations is less than 1.0×10^{-4}.

As the governing equations are valid in liquid, solid and mushy regions, there is no need to track the weld pool geometrical shape. Hence, a fixed-grid system was used in the numerical calculation. **Figure 2** shows the grid of the calculation domain. The time increment is 0.001 seconds and the calculation is terminated after 1.0 second from the start of the arc.

5. Results and Discussion

Figures 3(a)-(f) illustrate the velocity vectors (left), isothermal patterns (center) and streamline patterns (right) in the pure liquid and mushy regions for sulfur contents of 0.003%, 0.006%, 0.009%, 0.015%, 0.022%, 0.030% weight percent, respectively. Streamline associated with the counter-clockwise convection cell has a positive value and is plotted in equal increments between 0 and Ψ_{max}, while the clockwise convection cell has a negative value and is plotted in equal increments between Ψ_{min} and 0. Isotherms are plotted with 6 equal

increments between the minimum and maximum temperatures.

It can be seen from the velocity vector and streamlines plots in Fig.3(a) (left and right), that when the sulfur content in the material is 0.003% weight percent, the flow pattern has a clear and well developed circulation cell in a clockwise direction and a weak counter-clockwise circulation cell. In this situation high melting generally occurs near the cold corner of the pool, where warm fluid after being heated by the welding arc impinges on the semi-solid material in the mushy region. Then the fluid descends along the interface of solid/liquid and heat is transferred to the melting front, and results in the liquid temperature decreasing. Consequently, the melting rate at the base of the weld pool is lower than that at the cold corner of the pool surface. The weld pool profile revealed a relatively shallow and wide shape, similar to a 'shallow plan'.
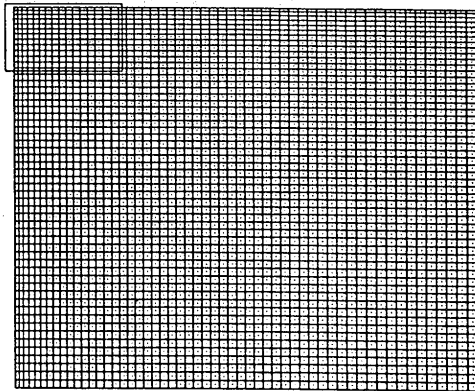
(a)
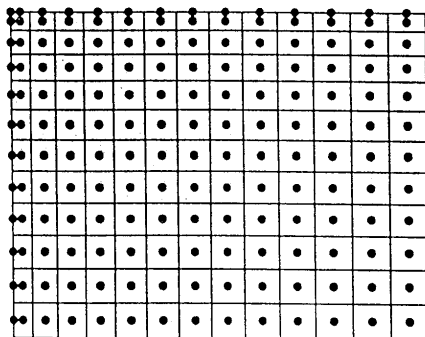
(b)

Fig.2 Grid mesh system for numerical simulation, (a) original grid mesh and (b) amplified local region to illustrate the detail at the surface nodes.

The flow pattern with two convection cells in each half of the weld pool is observed until the sulfur content reaches 0.015%. The counter-clockwise circulation adjacent to the cold corner of the pool is driven inward due to the presence of positive surface temperature coefficients. The clockwise circulation adjacent to the axis of the pool is driven outward due to the negative surface temperature coefficient. The inward flow collides with the outward flow at a certain region on the free surface of the pool. Then the flows in the two circulations join together after changing their direction and descend into the pool. This descending warm flow collides with the semi-solid front at the base of the pool where the flow transfers heat to the melting front. As a result, the weld pool is slightly deeper there, and relatively shallow at the center of the pool.

From the driving force point of view, the region with the positive surface tension coefficient on the weld pool surface is gradually extended with the increase of sulfur contents, and simultaneously the strength and size of the counter-clockwise cells are increased. Finally the flow in the weld pool consists of a strong cell accompanied by a weaker cell near the center of the pool as seen from the maximum and the minimum values of the stream function shown in Fig. 3.

When the sulfur content reaches 0.015%, the counter-clockwise cell occupies nearly the whole weld pool. This behavior becomes more clear with the increase of sulfur content. However, there is a rapid change for both the weld profile and the mushy region shapes as the sulfur content is increased from 0.009% to 0.015%. No substantial changes of the flow pattern take place from 0.022% to 0.030%. The reason is that the increase of sulfur contents would only enhance the strength of the counter-clockwise cell but can not change the fluid pattern.

Figures.3(a)-(f) (center) show the isotherms corresponding to the flows with sulfur contents ranging from 0.003% to 0.030% discussed in the preceding paragraph. It is also shown that the isotherms at a certain region in each half of weld pool are packed closer due to the clockwise flow, which carries high temperature fluid on the pool surface, colliding with the counter-clockwise flow, which has a lower temperature. Thus the surface tension gradient there is higher than that at both the center and the cold corner of the pool surface.

Figure 4 shows the surface temperature and tangential velocity distribution on the weld pool surface corresponding to Fig.3. It has been noted from the previous discussion that when sulfur content is 0.003%, there exists a clear clockwise cell occupying most of the weld pool and a weaker counter-clockwise cell near
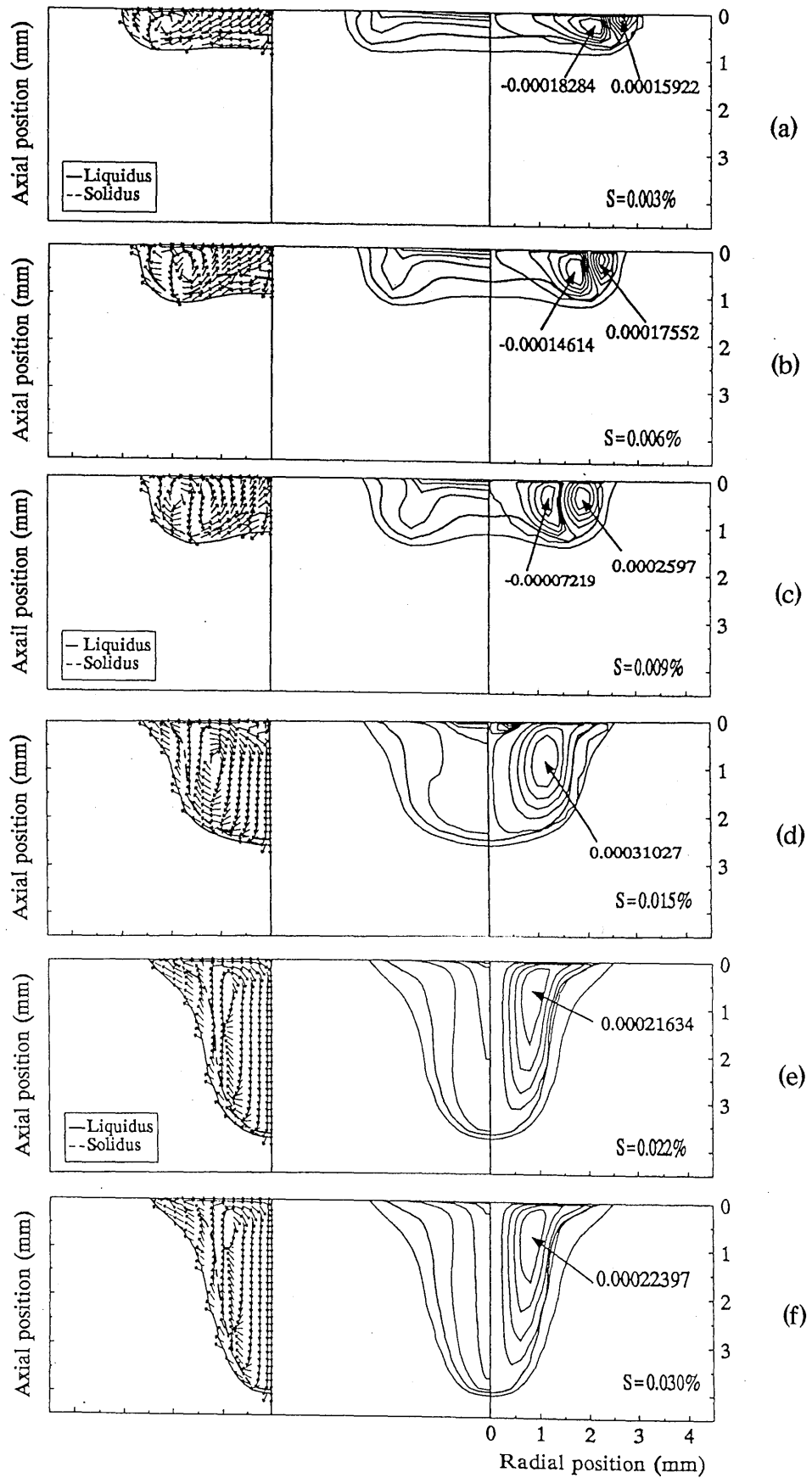
Fig.3 Calculated velocity fields (left), temperature isotherms (center) and streamlines (right) for different sulfur contents in the welded metal
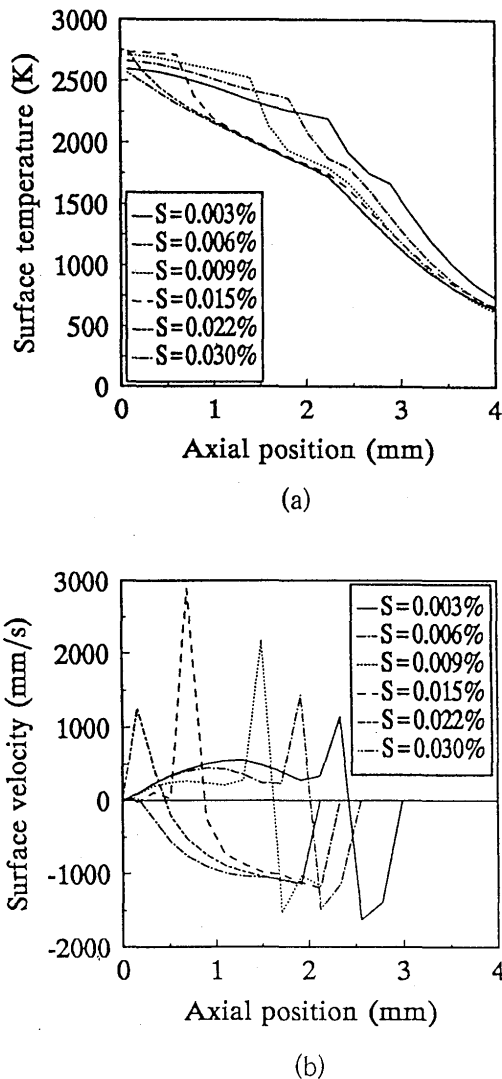
(a)

(b)

Fig. 4 Calculated surface temperature and velocity
distributions for the sulfur contents corresponding
to the Fig.3.

the mushy region. In this situation, the corresponding
surface temperature distribution given in Fig.4(a) has a
dramatic drop in the front of liquidus. Meanwhile, the
surface velocity profile has one peak value at that region
due to thermocapillary flow driven by a sharp temperature
gradient (see Fig.4(b)). With an increase in sulfur
content, the regions occupied by positive surface tension
temperature coefficients on the weld pool surface, and the
strength and area of the clockwise cell have been
increased. On the contrary, the region occupied by
negative surface tension temperature coefficients and the
size of the counter-clockwise cell have been decreased
(see Fig.3). The two groups of counter-directional flows
collide with each other at certain region on the pool
surface , and give rise to a great temperature gradient in

that region. This temperature gradient causes a peak value
of surface velocity at that region. It can be seen from
Fig.4(a) that the region where a deep drop of temperature
takes place approaches the center of the pool with an
increase in sulfur content. As a result, the position of the
peak value of surface velocity also moves inward toward
the axis of the pool. Viewing all of the curves
corresponding to each sulfur content, the peak values of
the surface velocity increase initially with an increase of
sulfur content, and reach maximum value of 2.9m/s at
0.022% S, and then the magnitude of the peak velocity
decreases gradually, reaching 0.3m/s when the sulfur
content increases to 0.03%.

6. Conclusion

(1) In view of the overall results, weld pool shapes and
penetrations are strongly affected by sulfur contents in
the weld. With an increase in sulfur content, the
strength and size of the fluid flow driven by the
positive surface tensions are increased and deep weld
penetration is produced.

(2) When the sulfur content is less than 0.009%, most
parts of the pool are occupied by clockwise
circulation. On the other hand, it is occupied by
counter-clockwise circulation when sulfur content is
above 0.015% .

(3) Two clear vortexes of opposite directions coexist in
each half of weld pool when sulfur content is in the
range from 0.003% to 0.015% weigh percent. One
located close to the centerline of the pool is
dominated by a negative surface tension gradient, and
the other locating near the mushy region at the corner
of the pool is induced by positive surface tension
gradients on the pool surface. These two circulations
have a strong influence on the weld pool profile.

(4) The width of the weld pool surface where the surface
tension gradient is less than or greater than zero
determines the size of the relevant circulation cell.
Therefore, the main factor determining the weld pool
profile is attributed to the width of the weld pool
surface where the sign of surface tension temperature
coefficient is positive or negative. The influence of
the absolute value of surface tension gradient is
relatively small.

(5) The collision of the two fluid flows in opposite
directions on the weld pool surface would give rise to
a greater gradient of surface temperature and result in a
peak surface velocity there. With increasing sulfur
content, the location of peak surface velocity
approaches the weld pool center, and the maximum
value of the peak surface velocity initially increases
and then gradually decreases and finally becomes zero.

References

1) T. Zacharia, A.H.Eraslan and D.K.Aidun, Modeling of non-autogenous welding, *Welding Journal,* Vol.67, 18s-27s, 1988

2) T. Zacharia, A.H.Eraslan, D.Aidum and S.A.David, Three-dimensional, transient model for arc welding process, *Mer. Trans.* B, Vol.20B. 645-659,1988

3) T, Zacharia, S.A.David, J.M.Vitek and T.Debroy, Weld pool development during GTA and laser welding of type 304 stainless steel, part 1   theoretical analysis, *Welding Journal,* Vol.68, 499s-509s, 1989

4) T, Zacharia, S.A.David, J.M.Vitek and T.Debroy, weld pool development during GTA and laser welding of type 304 stainless steel, part 2 - experimental correlation, *Welding Journal,* Vol. 510s-519s, 1989

5) K.Mundra, T.Debroy, T.Zacharia and S.A.David, Role of thermophysical properties in weld pool modeling, *Welding Journal,* Vol.71, 313s-320s, 1992

6) K.C.Tsao and C.S.Wu, Fluid flow and heat transfer in GMA weld pools, *Welding Journal,* Vol.67.70s-75s, 1988

7) H.G.Kraus, Experimental measurement of stationary ss304, ss316L and 8630   GTA weld pool surface temperatures, *Welding Journal,* Vol.68, 269s-279s, 1989

8) AKira Matsunawa, Marangoni effect in arc welding, *Materia Japan,* Vol.34 (4), 412-419, 1995

9) S.Kou and Y.H.Wang, Weld pool convection and its effects, *Welding Journal,* Vol.65, 63s-70s,1986

10) M.C.Tsail and S/Kou, Marangoni convection in weld pool with a free surface, *Int. J. Numer. Methods Fluid,* Vol9, 1503-1516,1989

11) M.C Tsai and S.Kou, Weld pool convection and expansion due to density variations, *Numerical Heat Transfer,* Part A, Vol.17, 73-89, 1990

12) M.E.Thompson and J.Szelaly, The transient behavior of weldpools with a deformed free surface, *Int. J. Heat & Mass Transfer,* Vol.32, 1007-1019,1989

13) R.T.Choo, J.Szelely and R.C.Westhoff, Modeling of high-current arcs with emphasis on free surface phenomena in the weld pool, *Welding Journal,* Vol. 69, 346s-361s, 1990

14) R.T.Choo and J.Szekely, Vaporization kinetics and surface temperature in a mutually coupled spot gas tungsten arc weld and weld pool, *Welding Journal,* Vol.71, 77s-93s, 1992

15) R.T.C.Choo, J.Szekely, and S.A.David, On the calculation of free surface temperature of gas-tungsten arc weld pool from first principles: Part 2, Modeling of the weld pool and comparison with experiments, *Met. Trans.* B, Vol. 23B, 371-384,1992

16) S.D.Kim and S.J.Na, Effect of weld pool deformation on weld penetration in stationary gas tungsten arc welding, *Welding Journal,* Vol. 71, 179-193, 1992

17) C.R.Heiple and J.R.Roper, Effect of element on GTAW fusion zone geometry. *Welding Journal ,* Vol.60, 143s-145s

18) C.R.Heiple and J.R.Roper, Mechanism for minor element effect on GTA fusion zone geometry, *Welding Journal,* Vol.61,97s-102s, 1982

19) C.R.Heiple and J.R.Roper, Effect of minor element on GTAW fusion zone shape. *Trends in welding research in the United States,* S.A.David, ed. American Society for Metals, Metals Park, Ohio, 489-520, 1982

20) C.R.Heiple and J.R.Porper, R.T.Stagner and R.J.Aden, Surface active element effect on the shape of GTA, Laser and electron beam welds. *Welding Journal,* Vol.62, 72s-77s, 1983

21) C.R.Heiple, P.Burgardt and J.R.Roper, The effect of trace elements on GTA weld penetration, *Modeling of casting and welding processes* 2, A.Dantzig and J.T.Berry, eds. TMA-AIME, Warrendale. Pa 193-205,1984

22) C.R.Heiple and P.Burgardt, Effects of SO_2 shielding gas additions on GTA weld shape. *Welding Journal.,* Vol.64, 159s-162s,1985

23) T.Hinata, K.Yasuda and Y.Kasuga, Study on penetration from using stationary GTA arc -- Study on low speed DC GTA welding method, *Transaction of the Japan Welding Society,* Vol.24 (2), 8-14,1993

24) P.R.Scheller, R.F.Brooks and K.C.Mills, Influence of sulfur and welding conditions on penetration in thin strip stainless steed, *Welding Journal.,* Vol.74, 1995

25) M.J.McNallan and T.Debroy, Effect of temperature and composition on surface tension in Fe-Ni-Cr alloys containing sulfur, *Met. Trans.* B., Vol.22B, 557-560, 1991

26) P.Shoo, T.Debroy and M.J.McNallan, Surface tension of binary metal-surface active solute systems under conditions relevant to welding metallurgy. *Met. Trans.* B., Vol. 19B, 483-491, 1988

27) Y.P.Lei and Y.W.Shi, Numerical treatment of the boundary condition and source terms on a spot welding process with combing buoyancy-Marangoni-driven flow, *Numerical Heat Transfer,* Part B., Vol.26, 455-471,1994

28) A. Block-Bolten and T.W.Eagar, Metal vaporization from weld pools, *Met. Trans.* B, Vol. 15B, 461-469,1984